MICROVASCULAR RESEARCH 10, 322–339 (1975)

Microvascular Hemodynamic Variations Accompanying[1] Microvessel Dimensional Changes

HARVEY N. MAYROVITZ, MARY P. WIEDEMAN,

Department of Physiology, Temple University School of Medicine, Philadelphia, Pennsylvania 19140

AND

ABRAHAM NOORDERGRAAF

Department of Bioengineering, University of Pennsylvania, Philadelphia, Pennsylvania 19174

Received April 7, 1975

The bat wing is used as an experimental preparation and as a self-contained vascular bed. The number, dimensions, and distribution of the vessels of the real vascular bed are included into an analyzable, representative geometric configuration. Based on theoretical analysis and experimental data, equations are developed and utilized to characterize the pressure–flow relationships for each branching order of the vascular field. The geometric configuration and associated describing equations are used to determine the effects of microvessel diameter change on the distribution of resistance, pressure, and velocity throughout the microvasculature. Predicted hemodynamic changes are compared with available experimental data and evaluated in the light of current concepts concerning the significance of microvessel dimensional changes.

INTRODUCTION

Peripheral vascular resistance is commonly calculated as the ratio between pressure difference across and flow through a vascular bed. Such calculated values have long been used as quantitative indices of the degree of vascular constriction or relaxation in a given bed. Though useful, such "macroscopic" calculations do not permit assessment of the relative contribution of the several branching orders of microvessels to blood flow resistance of the vascular network. On the other hand, microscopically observed changes in microvessels (Wiedeman, 1968; Baez, 1969; Intaglietta and Zweifach, 1971) that have provided unique information on normal and/or pathological changes of vascular regions have been interpretable neither in terms of the effect of such changes on vascular impedance nor in terms of microvascular hemodynamics.

Further progress in understanding information derived from such studies hinges on an extension of our understanding of the "microvascular–macrovascular" coupling.

Recognizing the inherent difficulties of a purely experimental approach, a few investigators (Intaglietta *et al.*, 1971; Lipowsky and Zweifach, 1974) have been able to utilize experimentally obtained data pertaining to vessel geometry and dimensions and certain

[1] Supported in part by SCOR-Thrombosis HL 14216.

hemodynamic aspects to develop mathematical models from which multifaceted interactions could be studied in proper perspective.

In the present paper, a mathematical model that characterizes the vasculature of and hemodynamics within the wing of the little brown bat is presented to gain insight into the influence of vascular dimensional changes throughout the wing vasculature on its hemodynamics. The general approach is to represent the number, dimensions, and distribution of vessels of the real vascular bed by a representative topological model. Each vessel of the topological model is then characterized by a resistance function that depends on the pressure–flow relationships applicable to that vessel. The ensemble of all such resistance functions are then used to calculate the resistance of the bed and the blood pressure and velocity distribution throughout the bed vasculature.

MODEL DEVELOPMENT

The bat wing vasculature is used as the experimental preparation for the model development. The topological and dimensional data of Wiedeman (1962, 1963) are utilized. In addition, the observed branching sequence of the main artery entering the wing, as well as a separation between arterioles and terminal arterioles, has been introduced.

Topological Properties

The numerical data contained in Table 1 form the basis for constructing the initial topological and architectural representation of the vasculature. To accomplish this, real vascular data are used, but some assumptions are made to develop a reduced but representative vascular structure. In the reduced version, the average vessel dimensions and branching distribution are maintained. The principal difference between the real topology and its reduced representation is the way in which arcuate vessels are represented. The reductions are as follows:

TABLE 1

VESSEL DIAMETERS, LENGTHS, AND AVERAGE NUMBER OF BRANCHES USED TO CONSTRUCT TOPOLOGICAL MODEL

Vessel	Diameter (μm)	Length (mm)	Number of branches
Main artery	97.0	40	13.0
Artery	52.0	17	12.0
Small artery	19.0	3.5	9.7
Arteriole	7.0	0.95	4.6
Terminal arteriole	5.0	0.20	3.1
Capillary	3.7	0.23	—
Postcapillary venule	7.3	0.21	—
Venule	21.0	1.0	5.0
Small vein	37.0	3.4	14.1
Vein	76.0	17.6	24.5

1. Small arteries arise only from arteries.
2. Arterioles arise only as side branches of small arteries.
3. Terminal arterioles arise only as extensions or branches of arterioles.
4. Capillaries arise as the final ramification of the terminal arterioles and terminate in postcapillary venules.
5. Postcapillary venules draining capillaries that have originated from the same parent terminal arteriole, drain into the same venule.

Reduction 1 is consistent with experimental observations. Reducation 2 excludes the possibility of arterioles emanating from any of the small arteries as a consequence of vessel dichotomous branching. Reduction 3 excludes the possibility of the arterioles

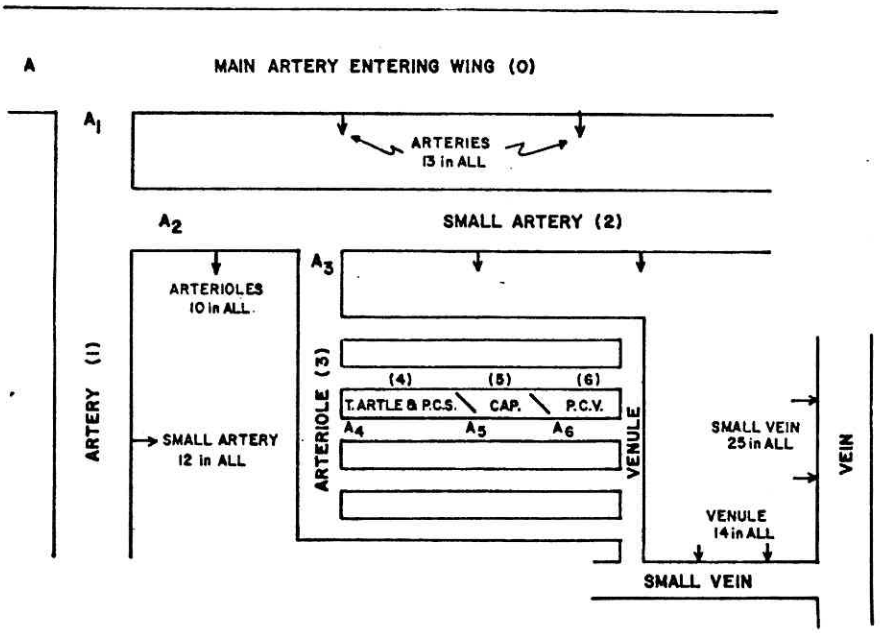

FIG. 1. Topological model. One pathway from main artery to small vein is shown in detail, and the remainder of the branches and vascular pathways are shown as straight arrows. Each vessels is given a name in accordance with those put forward by Wiedeman (1962), and in addition a branching order designation is shown in parentheses. The A's are used for reference to denote particular arteriolar sites. Dimensions and branching distribution are as given in Table 1. ARTLE = terminal arteriole, P.C.S. = precapillary sphincter, CAP. = capillary, P.C.V. = postcapillary venule.

forming arcades. Taken together, reductions 1, 2, and 3 means that the contribution of anastomoses between the small artery and arterioles to vascular resistance is not included in the topological model. The hemodynamic implications of arcuate patterns or arcades are unknown. However, Nicoll and Webb (1955) were of the opinion that the pattern serves a reservoir function and helps to maintain a uniform distribution of pressure throughout the arteries. If this is true, it would be expected that the hemodynamic effects of the arcades would be local and the effect on calculations of resistance would be of second order importance. Reduction 4 implies a single postcapillary venule per capillary. In Wiedeman's original work (Wiedeman 1962, 1963), all capillaries that took their origin from vessels other than arterioles were not counted as capillaries. The end of the capillary was defined as the point where an inflowing vessel joined it, the newly formed vessel being termed a postcapillary venule. When the total number of

vessels was tabulated, it was found that the number of postcapillary venules exceeded the number of capillaries counted by a factor of approximately 3. During the present observations, it could be seen that some of the joining tributaries were capillaries that arose as side branches from vessels not in the field of the single branch artery being studied; they are not included in the model. Reduction 5 does not appear unduly to restrict the generality of the analysis and is made to simplify the representation significantly.

A schematic representation of the topological pattern used to characterize and analyze the vasculature (which includes the preceding reductions) is shown in Fig. 1. It may be thought of as a "first generation" or topological model. Starting with the main artery at the top of Fig. 1, a single pathway is shown in detail, with the remaining pathways in the diagram represented by the large arrows. The number of branches is rounded to the nearest whole number. Adjacent to the name of each vessel type is a number in parentheses. This is for reference purposes and may be termed the vessel branching "order."

Hemodynamics

It now remains to describe the formulation of the pressure–flow equations utilized for each order of vessels defined by the topological model.

The generalized fluid equations frequently employed as a starting point are the Navier–Stokes equations together with the equation of continuity. Use of the Navier–Stokes relationships assumes the applicability of the concepts of continuum and homogeneity. In the microcirculation the blood is not homogeneous in any classical sense.

These difficulties notwithstanding, it is possible to obtain approximations that are useful in characterizing microcirculatory hemodynamics. These can be achieved by superimposing mathematical solutions obtained in regions in which the fluid dynamic equations are valid to an order sufficient for the purpose at hand and are dictated by the characteristics of the blood flow regime associated with a particular region of the vasculature or vessel type.

In the vasculature being analyzed there are several "types" of vessels, and as a consequence, there are several different mathematical formulations needed to represent pressure–flow relationships adequately. For example, in the analysis of the capillary longitudinal pressure drop, one approach is to solve hemodynamic problems that are applicable, respectively, to the plasma between cells (Fung, 1969; Lew and Fung, 1970) the deforming red blood cell (Barnard *et al.*, 1969; Lin *et al.*, 1973), and the peripheral plasma layer between the red blood cell and vessel wall (Lighthill, 1968; Fitz-Gerald, 1969). The separate solutions may then be combined (Mayrovitz, 1974) to characterize the total capillary arterial–venous pressure drop. The equations so obtained for one vessel type are solved simultaneously with the equations obtained for other vessels in the vascular network, both precapillary and postcapillary, to obtain a total solution.

The approach adopted here is to characterize each vessel in terms of an equivalent resistance defined as the ratio of pressure gradient to volume flow. Each of the vessels illustrated in Fig. 1 is then represented by its appropriate resistance functions on the basis of how it branches. Each vessel is represented by as many axial segments as there are branches, as shown in Fig. 2. Expressions are derived for the input resistance at any level of the vasculature as well as pressure and velocity distribution. The mathematical

formulations and developments have been detailed elsewhere (Mayrovitz, 1974) and are summarized in the following. Equations (1) through (5) are the hemodynamic analogs of classical network theory equations, the applicability of which is well documented (Noordergraaf, 1969). Equation (1) is used to calculate the resistance to blood flow at any branch point due to the vasculature distal to this point. When that branch point corresponds to the origin of a branch (e.g., as illustrated by A_1, A_2, etc., in Fig. 1). then Eq. (1) is reduced to Eq. (2) and is used to calculate the total input resistance seen looking into that branch from its parent vessel. Both Eqs. (1) and (2) as written are sufficiently general so as to account for vessel impedances. The resistance function specification of each vessel segment in the present analysis implies that both charac-

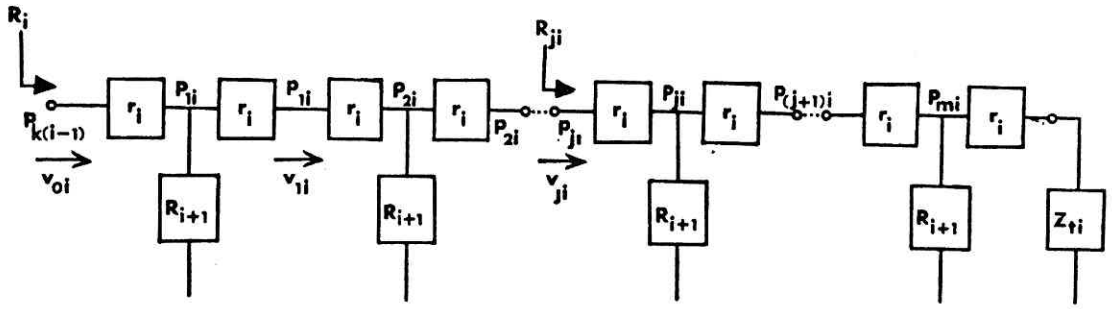

FIG. 2. Detailed representation of vessels. Each vessel of the topological model is represented by as many "T" sections as there are branches. This figure illustrates the general relationships for an ith order vessel; for example, if $i-2$, r_i represents the longitudinal resistance of the small artery (second order branch) and R_{i+1} the total resistance looking toward the capillary at each of the branching sites of the small artery, i.e., looking into the arteriole. The pressure at the origin, $P_{k(i-1)}$, is the pressure at the jth branch of the $(i-1)$ vessel (artery), and the pressure P_{ji} serves as the input pressure for the $(i+1)$ order vessels. The quantities R_{ji}, p_{ji}, and v_{ji} denote mean resistance, pressure, and velocity at the jth segment of the ith order vessel. The quantity R_i is the total resistance seen looking into the ith order vessel at its origin.

teristic impedance and terminating impedances (and hence their ratio, ρ) are real functions with no imaginary parts. Equation (3) expresses the spatial pressure distribution along a vessel in terms of the pressure at the origin of the vessel and together with Eq. (4) permits calculation of the pressure at any branch point. Equation (5) is used to calculate the blood velocity in any vessel segment (as illustrated in Fig. 2) and is seen to be determined by the volume flow entering that segment (p_{ji}/R_{ji}) and the cross-sectional area of the segment in question. The longitudinal resistance (r_i) of the set of ith order vessel segments as given by Eq. (6) enter into the determination of the resistance, pressure, and velocity distribution expressed by Eq. (1) through (5) via the propagation constant γ_i. In the analysis presented here, a hematocrit value of 35 is used. Based on the *in vitro* studies of Barbee and Cokelet (1971), this hematocrit value in the artery entering the wing corresponds to a hematocrit of about 43 for the blood feeding this vessel. This value is consistent with normal whole blood hematocrit values. Further reductions in hematocrit with decreasing vessel diameter as demonstrated *in vitro*, for example, by Barbee and Cokelet (1971) are not included for vessels having diameters greater than the RBC undistorted diameter ($\nu < 1$). For vessels smaller than the RBC diameter ($\nu \geq 1$), local hematocrit is dependent on the ratio of plasma velocity to red blood cell velocity as well as the hematocrit of the supplying vessel. Inclusion of this relationship

shows for example that a 7-μm arteriole (Table 1) may have a local hematocrit of 21.5 (for a systemic hematocrit of 43) and a capillary hematocrit of 10. The average red blood cell axial separation (β) is taken as uniform in a given vessel and calculated from the local hematocrit on the basis of a red blood cell volume of 61 μm^3 and a distorted axial length of 3.1 μm. The dimensionless red blood cell to vessel diameter ratio (ν) is determined on the basis of a 7.5-μm red blood cell diameter. Yield stress (τ_y) and plasma viscosity (η_p) are 0.04 dynes cm^{-2} and 0.013 Poise, respectively, in the present calculations.

EQUATIONS

i = index denoting vessel branching order.
j,k = indices denoting specific branches or vessel segments.
m_i = number of segments used to represent each ith order vessel.
= number of branches of the ith order vessel.
r_i = longitudinal hydraulic resistance of each ith order vessel segment.
R_{ji} = total resistance seen looking into the jth segment of an ith order vessel.
R_{in} = total input resistance seen looking into an ith order vessel at its origin.
$P_{k(i-1)}$ = mean blood pressure at the kth branch of an $(i-1)$ order vessel.
= pressure at the origin of an ith order vessel.
P_{ji} = mean blood pressure at a jth branch of an ith order vessel.
= pressure at the origin of an $(i+1)$ order vessel.
p_{ji} = mean blood pressure at the jth segment of an ith order vessel.
V_{ji} = mean blood velocity entering the jth segment of an ith order vessel.
γ_i = propogation constant of an ith order vessel.
= $\cosh^{-1}\{1 + [r_i/(R_{i+1})]\}$.
Z_{ci} = characteristic impedance of an ith order vessel.
= $[r_i(r_i + 2R_{i+1})]^{1/2}$.
Z_{ti} = terminating impedance of the mth segment of an ith order vessel.
ρ_i = ratio of characteristic to terminating impedance.
= Z_{ci}/Z_{ti}.
l_i = average length of ith order vessel.
D_i = average diameter of ith order vessel.
η_p = plasma viscosity.
ν = ratio of undistorted red blood cell diameter to vessel diameter.
β = ratio of average red blood cell separation to vessel diameter.
H = local hematocrit ($H < 1$).
τ_y = blood yield stress.
p' = local pressure gradient.
σ = a parameter = $\tau_{y/D}/p'$.
$F(\sigma)$ = $1 - (32/7)\sigma^{3/2} + (16/3)\sigma - (4/21)\sigma^4$.
K = a constant = 1.14.

$$R_{ji} = Z_{ci}\left\{\frac{\rho_i \sinh(m_i - j) + \cosh(m_i - j)\gamma_i}{\sinh(m_i - j)\gamma_i + \rho_i \cosh(m_i - j)\gamma_i}\right\} \quad i = 0, 1, 2, 3\ldots, \quad j = 0, 1, 2, 3\ldots, m_i. \tag{1}$$

$$R_{in} = Z_{ci}\left\{\frac{\rho_i \sinh m_i\gamma_i + \cosh m_i\gamma_i}{\sinh m_i\gamma_i + \rho_i \cosh m_i\gamma_i}\right\} \quad i = 0, 1, 2, \ldots. \tag{2}$$

$$P_{jl} = P_{k(l-1)} \left\{ \frac{\rho_l \sinh (m_l - j)\, v_l + \cosh (m_l - j)\, v_l}{\cosh m_l \gamma_l + \rho_l \sinh m_l \gamma_l} \right\} \qquad i = 1, 2, 3\ldots,$$

$$j = 0, 1, 2\ldots, m_l \qquad k = 1, 2, 3, \ldots, m_{l-1}. \tag{3}$$

$$P_{jl} = [p_{jl} + p_{(j+1)l}]/2. \tag{4}$$

$$v_{jl} = (4p_{jl})/(\pi D_l^2 R_{jl}). \tag{5}$$

$$r_l = \frac{64\eta_p l_l}{\pi D_l^4 m_l} \left\{ \left[1 + \left(\frac{v}{4}\right) + \left(\frac{v}{4}\right)^4 \right] (2 - e^{-k/v})(1 + 0.6e^{-\beta}) \right\} \qquad v \geqslant 1. \tag{6}$$

$$= \frac{64\eta_p l_l}{\pi D_l^4 m_l} \left(1 + 2.5 \frac{H}{1 - H} \right) F(\sigma) \qquad v < 1.$$

METHOD OF ANALYSIS

The dimensions of individual vessels listed in Table 1 are taken as reference values and used to calculate control values for input resistance, pressure, and velocity distribution. All arterial vessel diameters of a given branching order are then changed according to two protocols:

1. To determine the effect of changes intrinsic to a single branching level, each diameter is varied independently, while all others are maintained at their control values. The resultant information is termed "individual vessel effects."

2. To determine the interactive effects due to simultaneous variation in vessels of a different branching pattern, multiple vessel dimensional changes are made and resultant hemodynamic quantities are calculated. An illustrative sequence is to compare the effects of fourth order vessel diameter change to the effects of equal fractional diameter changes in (a) both fourth and third order vessels, (b) fourth, third, and second order vessels, and (c) all vessel orders. The information obtained from this analytical protocol is termed "composite vessel effects."

RESULTS

Except as noted, all graphical results are presented in normalized form for convenience and ease of generalized interpretation. D will represent the vessel diameter, and D_c its control value. The maximally dilated vessel diameter is D_{max} and is taken as twice D_c. Vessel diameters are normalized either to their respective control diameters as D/D_c or to their maximally dilated value as D/D_{max}. The hemodynamic quantities (pressure, resistance, and velocity) are normalized to their respective value as calculated for the control case or for the maximally dilated state.

Variation in Diameter of Individual Vessels

Figure 3 is a composite plot illustrating the functional relationship between independent changes in vessel diameter and the effect of these changes on the input resistance (as seen at site A, Fig. 1) of the vascular bed as calculated using Eq. (2). The comparatively larger influence on the input resistance to changes in the larger diameter vessels than to the smaller diameter vessels is a characteristic that is quite apparent. Thus, for example, a reduction in the first order vessel diameter (ΔD_1) to 50% of its

control value produces a 1.5 times as much change in input resistance as an equal fractional change in fourth order vessels. By taking the change in input resistance produced by halving and doubling, the fourth order vessel diameter as unity, we may express the changes in input resistance due to any other branching order in terms of the fourth order vessel effects. As shown in Fig. 4, the relative effect on input resistance is

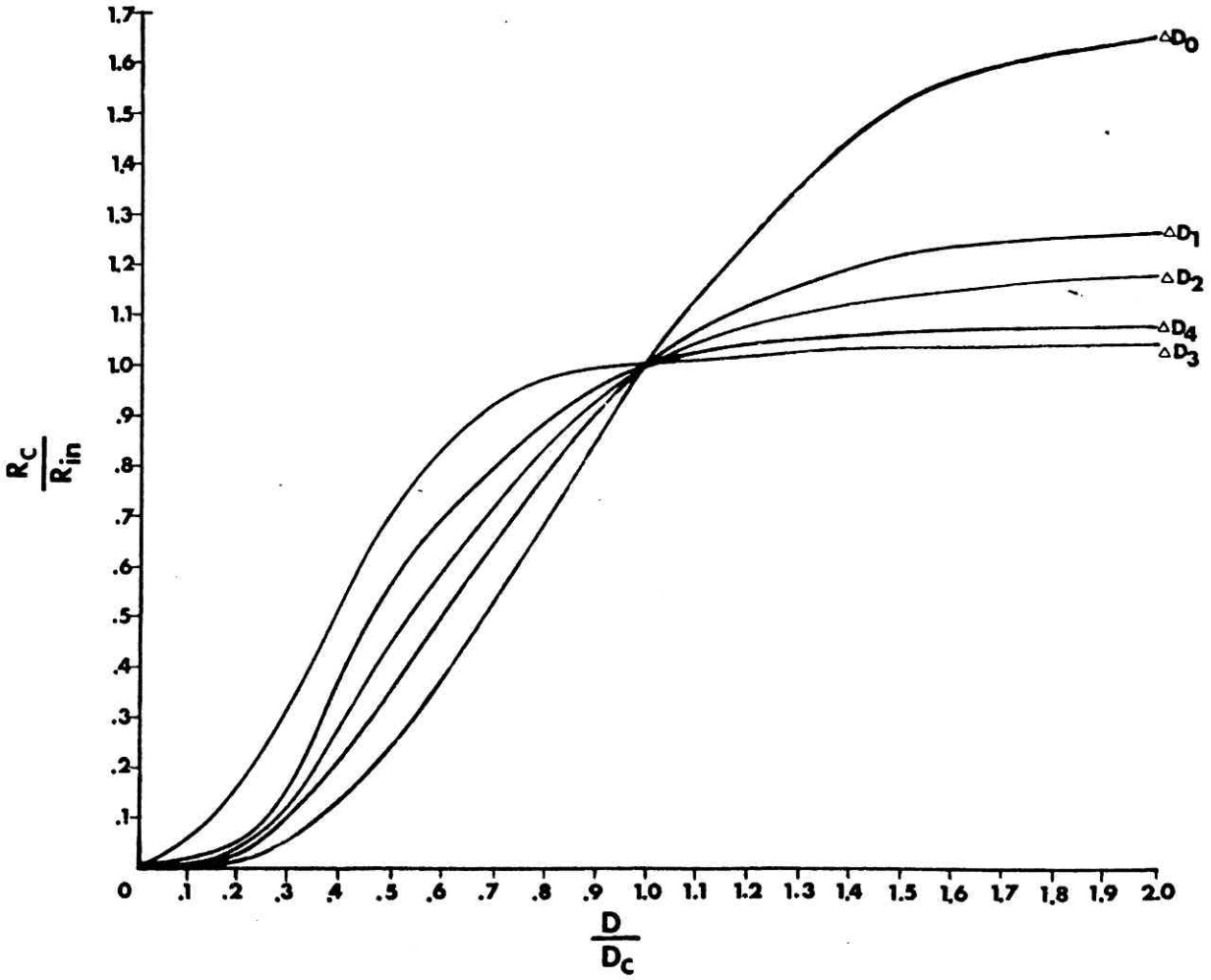

FIG. 3. Normalized bed input resistance (as seen at site A, Fig. 1) as a function of diameter of individual vessel orders. Each curve represents the change in resistance due to change in one branching order while other dimensions are held constant. Resistance and diameters are normalized to control values R_c and D_c as R_c/R_{in} and D/D_c. Thus, ΔD_0, ΔD_1, ΔD_2, ΔD_3 and ΔD_4 correspond to changes in diameter of the zero order through fourth order branches, respectively.

quantitatively larger for contraction than for dilation with the exception of the third order vessel effects, for which the converse is true.

Figure 5 illustrates the effect of individual and independent diameter changes on the proportion of main artery pressure at the entrance to a terminal arteriole (fourth order branch) and in the capillary that it serves. As may be noted, for the arteriole, the control value of pressure ($D = D_c$) at this particular site is 67% of that in the main artery that serves this vessel. For an arterial mean pressure of 90 mmHg, the pressure in the arteriole is about 60 mmHg. For diameters less than control, pressure at this arteriolar site is seen to increase only with decreasing fourth order vessel diameter. For diameter

values larger than control, however, changes in second order branches are seen first to increase slightly and then decrease arteriolar pressure, whereas dilation of third and fourth order branches monotonically increase and decrease it, respectively.

The bimodel characteristic illustrates the fact that changes in vessel diameter of a single branching order produce two opposite effects with respect to pressure within a distal branching order. For example, dilation of second order branches will reduce the pressure loss through second order vessels and will tend to increase pressure at distal sites. However, the same second order dilation will also reduce the input resistance as seen by the first order vessel, thus increasing the pressure loss up to the second order branch site. Thus, to a given geometrical and dimensional distribution throughout

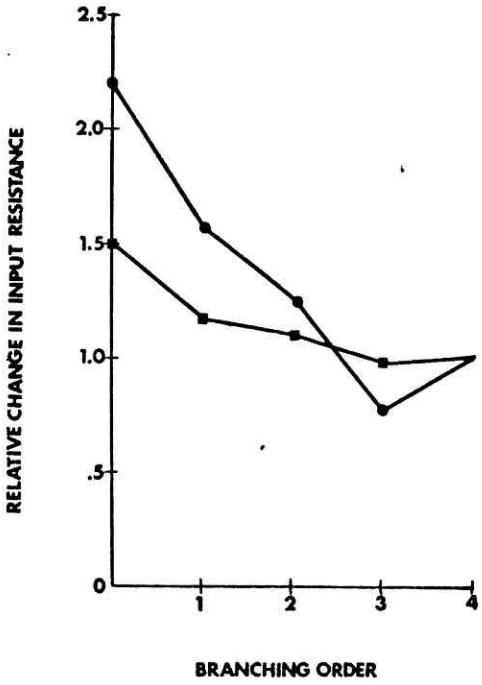

FIG. 4. Relative change of input resistance due to changes in diameter of different branching orders. The circles denote the relative change in input resistance due to halving the control diameter (contraction), and the squares denote doubling (dilation) the vessel diameters. The relative effect is expressed as the ratio of the change caused by a given branching level, relative to that produced by fourth order vessels.

the vascular bed, there is a corresponding maximum in the pressure transmission ratio. From the quantitative point of view, it should be noted that it takes only 15% contraction from control of the fourth order vessel to produce an increase in arteriole pressure in excess of that possible with full dilation of the vessels upstream from this site. The quantitative effect of these fourth order vessel changes on proximal capillary pressure is shown in the bottom part of the figure.

Composite Vessel Effects

Input resistance. In Fig. 6 the effect on bed input resistance of equal fractional changes in diameter of multiple branching levels is illustrated. The maximally dilated vessel diameter is twice the control value, and the input resistance calculated at this level is minimal (R_{min}). Reduction in vessel diameter (decrease in the normalized ratio D/D_{max}) causes a decrease in the ratio R_{min}/R_{in}.

It should be noted that constriction of a vessel is associated with a monotonic increase in input resistance. For equal fractional diameter reductions, the incremental increase in the input resistance goes up as the number of vessels that constrict increases. For example, a 50% reduction in both fourth and third order vessels produces a 12% change in input resistance, whereas the same fractional change in diameter of fourth, third, and second order vessels produces a 28% change in resistance. Also note that the

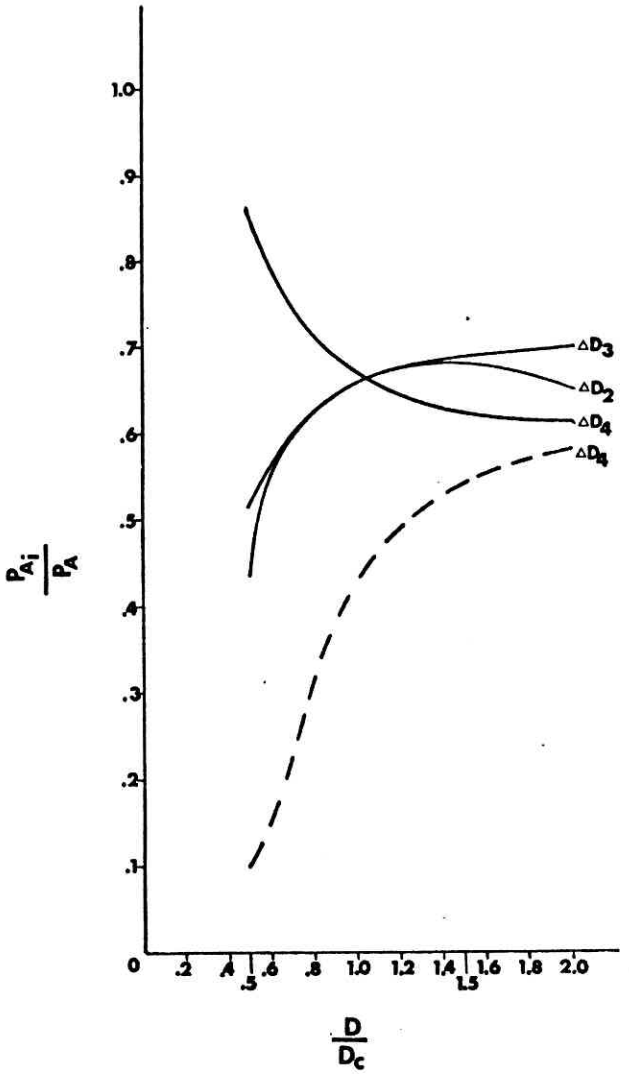

FIG. 5. Diameter-induced change in the fraction of arterial pressure (P_{A_i}/P_A). Solid curves show change in pressure at arteriole site (A_4) caused by fractional changes in diameter of second (ΔD_2), third (ΔD_3), and fourth (ΔD_4) order vessels. Dashed curve shows change at proximal capillary site (A_5) due to change in fourth order vessels.

predicted sensitivity of input resistance to diameter change (curves A through D) is considerably different from that which would be obtained by assuming a strict $1/D^4$ dependence (curve E) as is so often done.

Pressure distribution. The changes in the pressure distribution throughout the vascular bed accompanying changes in vessel diameter are illustrated in Figs. 7 and 8.

It can be seen that in each case the pressure decreases toward the capillary. The net effect shows that whether all vessels change dimension (Fig. 8) or a single type of vessel

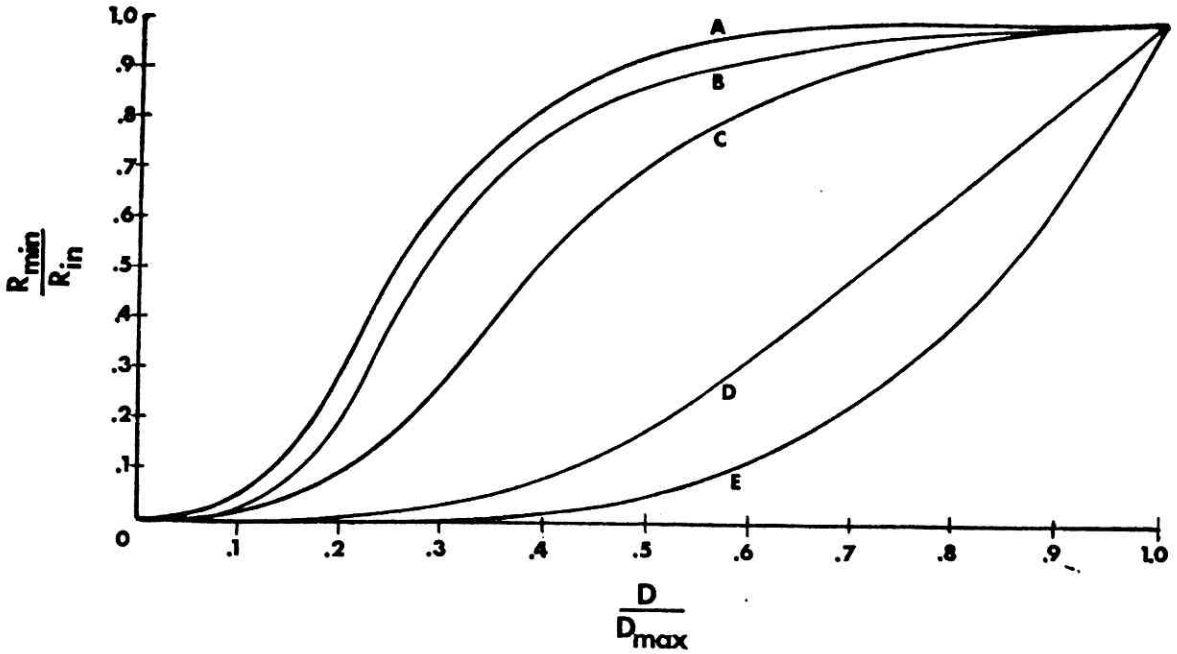

FIG. 6. Normalized bed input resistance (as seen at site A in Fig. 1) as a function of fractional diameter changes of multiple branching orders. Resistance and diameters are normalized to maximally dilated values, respectively, as (R_{min}/R_{in}) and D/D_{max}. Thus, when $D = D_{max}$, then $R_{in} - R_{min}$, and each normalized ratio is unity.

Curve A: change in fourth order vessels; curve B: change in third and fourth order vessels; curve C: change in second, third, and fourth order vessels; curve D: change in all vessels; curve E: calculated on the basis of $1/D^4$ dependence of vessel resistance.

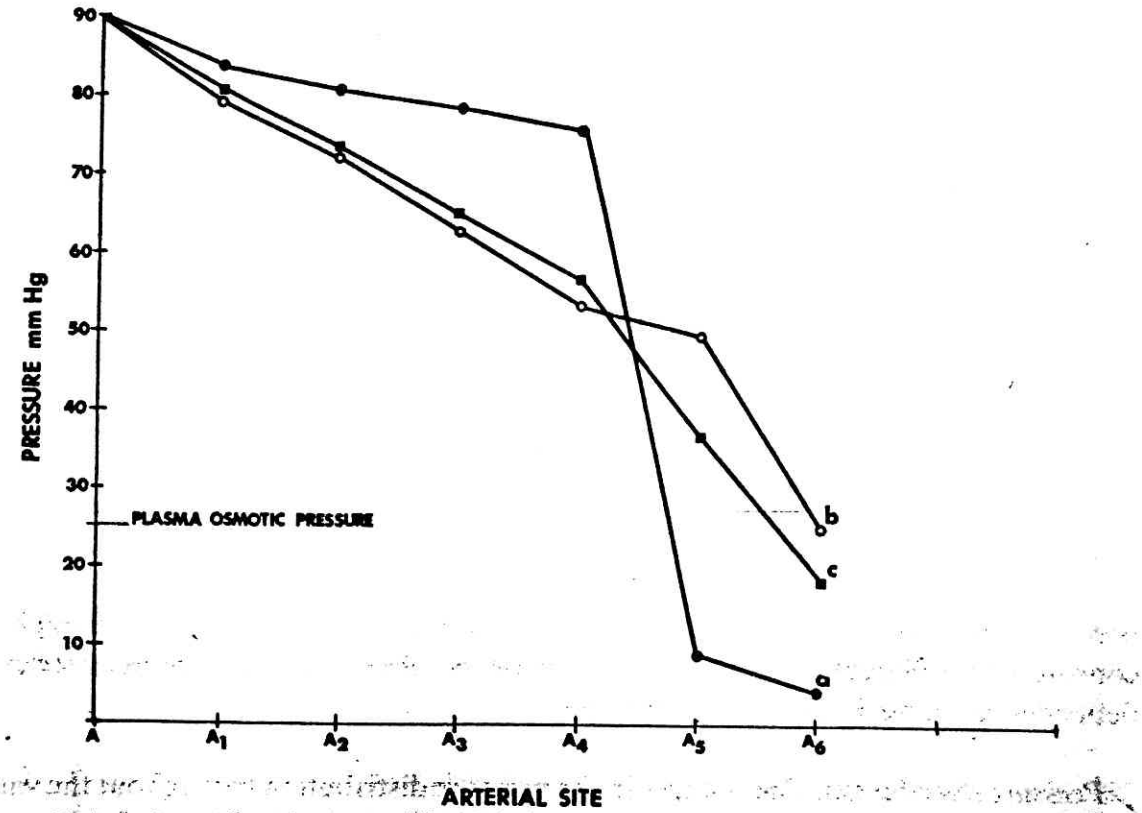

FIG. 7. Pressure distribution in the vasculature and its change due to alteration in diameter of fourth order branching vessels. Curve c: control dimensions; curve b: vessels contracted (one-half control); curve a: vessels dilated (twice control).

changes (Fig. 7), the capillary pressure increases with vessel dilation and decreases with vessel contraction. However, several significant differences between fourth order vessel changes alone and changes in all vessels may be observed.

Considering first the effect of vessel contraction (curve a), we see that for fourth order vessel changes only (Fig. 7), the pressure upstream from the proximal capillary site (A_5) is greater than the control case (curve c). Contrastingly, if all vessels contract (Fig. 8), the pressures are everywhere less than the control values. For vessel dilation,

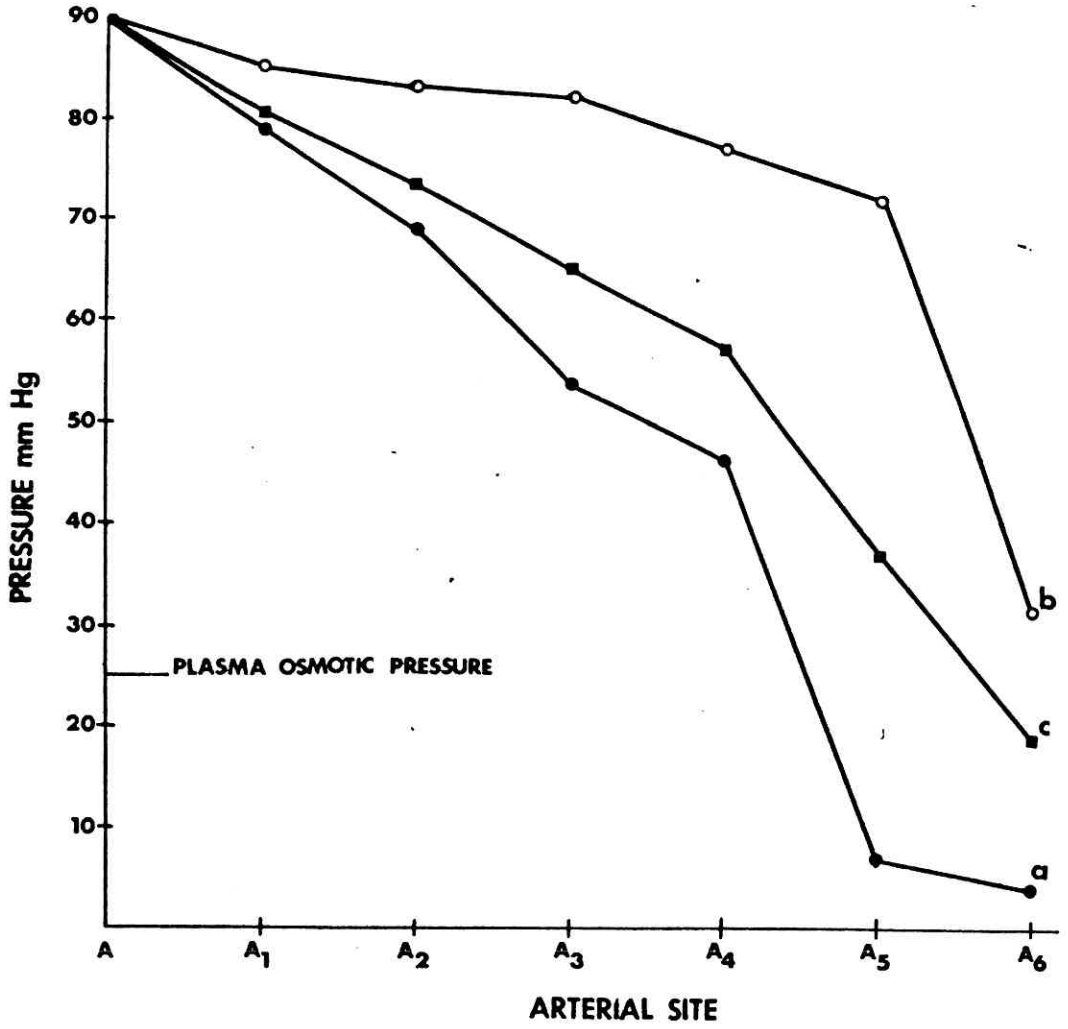

FIG. 8. Pressure distribution in the vasculature and its change due to alteration in diameter of all branching orders. Curve c: control dimensions; curve b: vessels contracted (one-half control); curve a: vessels dilated (twice control).

the converse of this is true. These directionally opposite upstream pressure changes notwithstanding, it can be seen that the pressure at the proximal capillary site (A_5) and distal capillary site (A_6) change in the same direction as the diameter changes whether one or all vessel orders are involved.

The magnitude of this pressure change and hence the quantitative effect on capillary filtration properties would appear to be quite large. If we accept the classical value of 26 mmHg as the "average" capillary osmotic pressure, thus in a straightforward fashion, the calculations show that in the control state the first two-thirds of the true capillary is associated with bulk filtration, while the final third and the entire post-

capillary venule are associated with the net absorption. When the fourth order vessels dilate and elevate capillary pressure, the result is filtration through the capillary that has zero filtration over its entire length. When all vessels are involved, results are similar, but because of the magnitude of the changes in capillary pressure, the effects are larger.

Figure 9 shows the predicted change in pressure distribution associated with denervation of the wing. Acute denervation was found to increase the diameters of vessels upstream from the third order branching level and decrease the diameters of third and

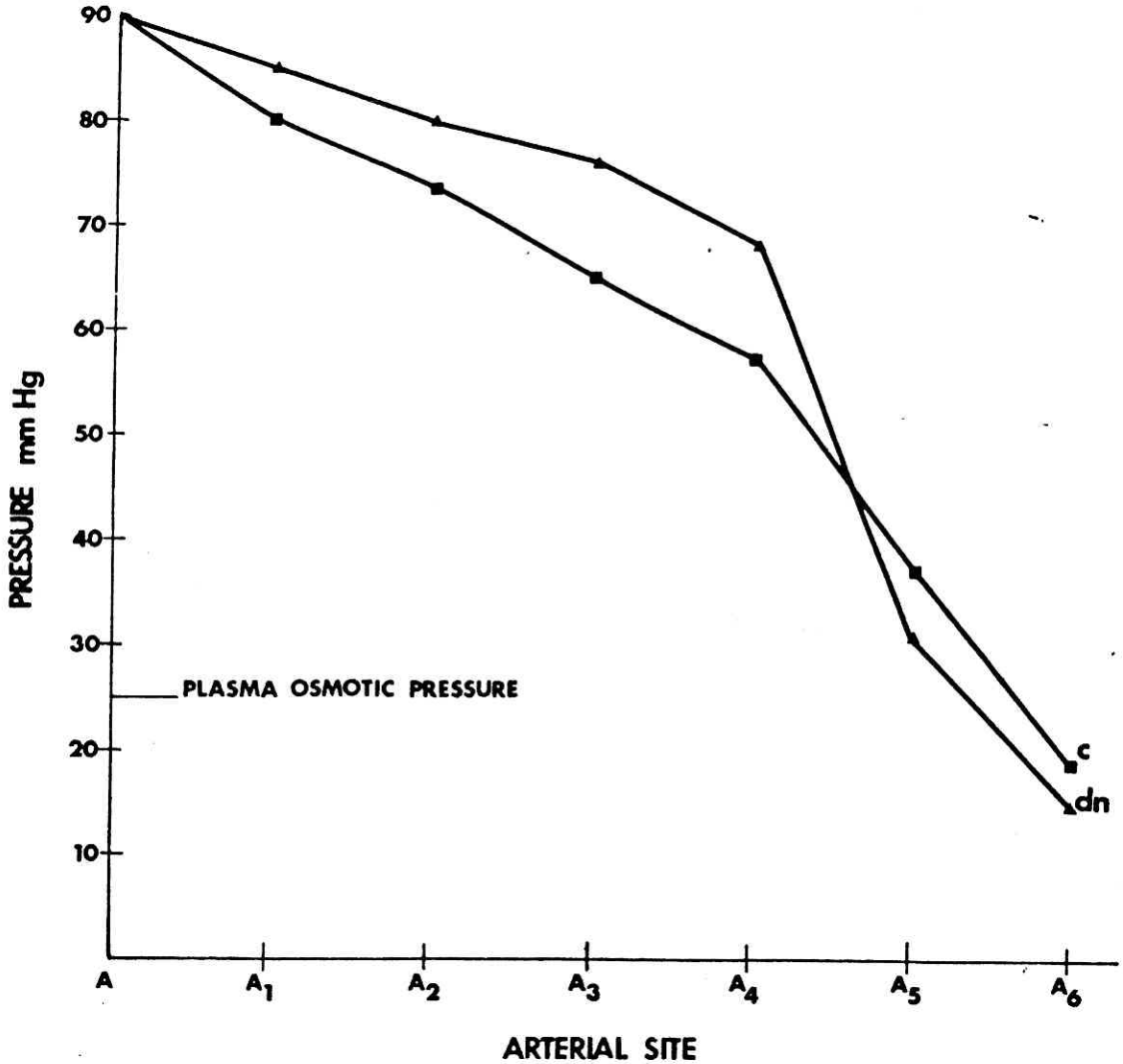

FIG. 9. Pressure distribution in the vasculature and its change due to denervation. Curve c: control curve; dn: denervation.

fourth order branches (Wiedeman, 1968). The effect of this bimodal vascular response is to increase the pressure relative to control in the larger vessels but to decrease it slightly at the capillary level. The net change on the effective capillary exchange gradient is small but does result in a slight shift in the spacial location of the point at which osmotic and hydrostatic forces balance.

Velocity distribution. Figure 10 illustrates the velocity distribution as calculated for the control state and as modified by equal fractional changes in third and fourth order dimensions.

Comparison of the velocities associated with the control and contracted states shows that the consequence of combined third and fourth order contraction is a reduction in velocity at every branching order. Dilation of these vessels causes increase in velocity

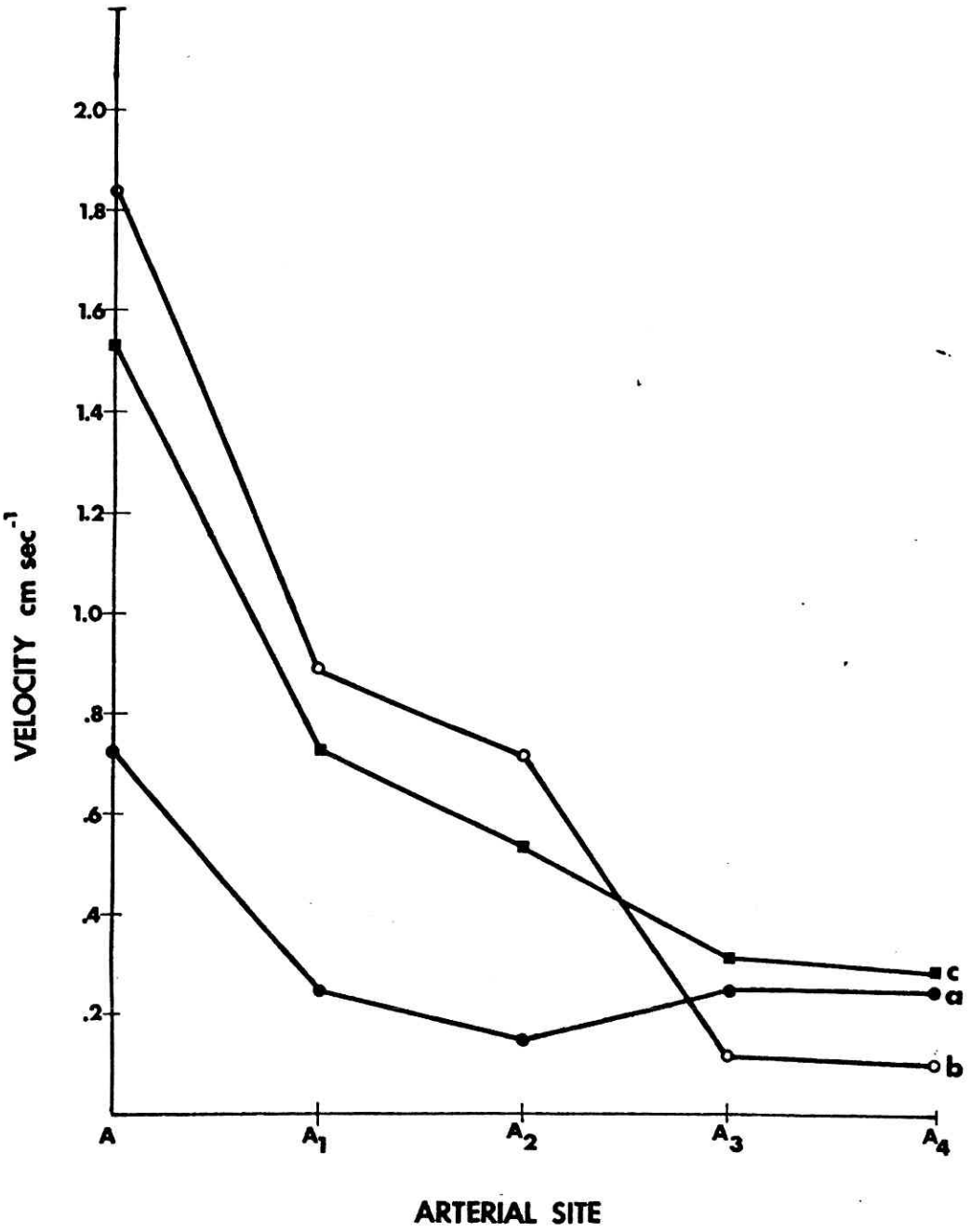

FIG. 10. Mean velocity distribution in the vasculature and its change due to equal fractional changes in diameter of third and fourth order branching vessels. Curve c: control dimensions; curve b: vessels dilated to twice control; curve a: vessels contracted to one-half control.

in vessels that are upstream from the third order branch but decrease (as compared with control) in the contracted vessels themselves. These velocity characteristics illustrate the interactive effects of microvascular and macrovascular aspects. As was shown in Fig. 3, contraction of third and fourth order vessels results in increase in vascular bed input resistance. Under the assumption of intact arterial pressure control, the

sequel is a decrease in total vascular inflow. In those branching order levels in which no dimensional changes occur (0, 1, and 2), velocity will unquestionably decrease. At the third and fourth order branching level however, the amount and direction of velocity change depends on the relationship between the total input flow reduction and flow distribution caused by the diameter change of the constricting vessels. For example, a 50% reduction in third and fourth order vessel diameter will decrease the total inflow by 66%. However, because of the vascular topology, the percentage of flow reduction in each of the branches of a given parent vessel will not be uniformly reduced by this factor. The velocity in a given contracting branch may decrease, remain unchanged, or possibly increase by an amount that is calculable as determined by the amount of diameter change as well as its hierarchial position in the vascular tree. For the vascular sites illustrated in Fig. 10, all velocities are seen to decrease.

Again with reference to Fig. 10, it can be seen that dilation is associated with velocity increase in vessels upstream from the dilated vessels. But as was the case for the contracted state, in the third and fourth order vessels, where vessel dilation is an increase in total bed input flow, the nonuniform change in the branch flow distribution coupled with the increase in vessel diameter produces a decrease in small vessel velocity.

DISCUSSION

The basic motivation for the development of this model was to provide a cohesive framework from which it would be possible to interpret interactive facets of microvascular–macrovascular coupling. As with most mathematical models of complex biological processes, certain initial simplifications are introduced to make the problems dealt with tractable.

At this time, there is no indication that any of these simplifications substantially alter the fundamental results and predictions obtained. These results relate specifically to the effect of microvessel diameter change on hemodynamic quantities throughout the wing vasculature. The principal focus of interest may be conveniently separated into (1) effects on pressure, (2) effects on velocity, and (3) effects on vascular bed input resistance.

Pressure Distribution

The distribution of mean pressure throughout the bed in a quiescent state (e.g., Fig. 7) qualitatively agrees with standard textbook representations (Folkow and Neil, 1971; Henry and Meehan, 1971) and, more significantly, is quantitively comparable to recent *in vivo* measurements in the bat wing by Wiederhielm and Weston (1973). They found mean arterial capillary pressure to be 32 mmHg (model prediction is 37 mmHg) and venous capillary pressure to be 16 mmHg (model prediction is 18 mmHg). These mean values were subject to wide variation that, according to the authors, was associated with precapillary sphincter activity. Since this activity is simulated in a quasi-static mode in the model (dilation and contraction of fourth order vessels), it is of significance to compare the experimentally recorded extremum values at each capillary end with those obtained theoretically. This comparison reveals that in both the experimental and theoretical cases, contraction and dilation of the fourth order vessels result, respectively, in a reduction below and an elevation above the assumed level.

of plasma colloid osmotic pressure. The quantitative significance of the dynamic aspects of such precapillary activity on classical concepts of capillary exchange and local hemodynamics has been reported previously (Mayrovitz *et al.*, 1973). However, the point emphasized here is that via the use of the model, in which both macrovascular and microvascular effects may be seen, the fourth order diameter modulation is, by itself, a powerful controller of capillary hemodynamics.

The present results also have a bearing on the question of the extent to which neural factors influence capillary status. As shown in Fig. 9, complete removal of nervous input to the vascular bed studied, though altering upstream pressures, only slightly altered the filtration status of the capillary, even though the total inflow to the bed (as calculated from the decrease in input resistance) increased by 58 %.

Velocity

In 1970 (Gaehtgens *et al.*) data were presented indicating that a strong correlation between vessel dimension and red blood cell velocity could be demonstrated if velocity measurements were made systematically within a well-defined vascular segment. The bat wing, for which the present results are most directly applicable, is characterized by a topology that is well defined, and hence it might be expected that the velocity distribution across the vascular bed should display a similar correlation. As shown in Fig. 10 for the control state, the wing displays an arterial blood velocity distribution that decreases as branching increases. However, this monotonic relationship need not hold for all vascular states. For example, as shown by Fig. 10 (curve a), the velocities in third and fourth order branches are greater than those in the second order branch. This condition occurs when the peripheral vessels, either singly or in combinations, are constricted to produce a reduction in total wing flow. We conclude that velocity measurements made in individual vessels (and changes in these velocities) at a given position depend not only on the dimensional properties of the vessel being studied but also on the relationship between their dimensions and those of each of the branching vessels contained in the vascular bed under consideration. These facts again emphasize the need to interpret localized microvascular hemodynamic measurements carefully in the context of their interdependency on overall vascular topology, dimensions, and dynamics.

Resistance

Change in vessel diameter is a principal mechanism for adjustment of total flow to, and distribution within, a given vascular bed. In addition, pathological vascular changes are basic factors in the etiology of clinical circulatory problems such as peripheral vascular disease and essential hypertension. A question of long standing is to what extent vascular resistance is dependent on the vessels associated with different branching levels. By examining the effect of diameter changes in each division of vessels, it has been possible quantitatively to predict the effects. The intrinsic sensitivity of vascular input resistance to vessel diameter change is shown to decrease with increasing branching order (Figs. 3 and 4). Differences in effect due to consecutive branching levels depend on whether diameter increments are positive or negative with respect to control dimensions as well as on the magnitude of the diameter change. The

interrelationships are quite nonlinear and bear little resemblance to characteristics deduced from serial models of the vascular bed.

Though possible, it is unlikely that under normal conditions, physiological and/or pathological processes will result in vessel diameter changes at only one branching level. As might have been intuitively reasoned, the results obtained (Fig. 6) show that increasing the number of vessel orders involved in dimensional changes produces a progressive increase in the summated effect on input resistance. Perhaps more significantly however, is the fact that the increment in input resistance produced by increasing participation of branching orders depends in a nonlinear (but calculable) fashion on the number of branching levels involved as well as on the diameter of the vessels considered. These facts again point up the inappropriateness of characterizing bed resistance by a D^{-4} dependence, as is so often done on the basis of the assumed applicability of Poisuille's law.

With the exception of simultaneous changes in dimensions of all branches, the shapes of the resistance-vs-diameter curves are comparable to those experimentally determined by Folkow *et al.* (1972) in their studies on the spontaneously hypertensive rat. Each of the curves (Fig. 6) displays a threshold and saturation (maximally dilated resistance value) as defined by these authors, who believe that at least part of the hypertensive character of these animals is due to effective arteriolar diameter reduction associated with vascular wall hypertrophy and enhanced reactivity. An alternate hypothesis, stemming from the experimental findings of Hutchins *et al.* (1973), who found no increased small vessel reactivity, is that the decrease in the number of arterioles principally accounts for the hypertensive status.

An unanswered question, then, is whether a normal vascular bed when altered topologically and dimensionally as reported will display resistance-vs-diameter properties that are characteristic of the spontaneously hypertensive rat. The present model is suited to the attack on this problem.

REFERENCES

BAEZ, S. (1969). Simultaneous measurements of radii and wall thickness of microvessels in the anesthetized rat. *Circ. Res.* **25**, 315–329.

BARBEE, J. H., AND COKELET, G. R. (1971). The Fahraeus Effect. *Microvasc. Res.* **3**, 6–16.

BARNARD, A. C., LOPEZ, L. AND HELLUMS, J. D. (1969). Basic theory of blood flow in capillaries. *Microvasc. Res.* **1**, 23–34.

FITZGERALD, J. M. (1969). Mechanics of red-cell motion through very narrow capillaries. *Proc. Roy. Soc. London Ser. B* **174**, 193–227.

FOLKOW, B., AND NEIL, E. (1971). "Circulation," p. 7. Oxford Univ. Press, London and New York.

FOLKOW, B. HALLBÄCK, M., LUNDGREN, Y., AND WEISS, L. (1972). The effects of "immunosympathectomy" on blood pressure and vascular "reactivity" in normal and spontaneously hypertensive rats. *Acta Physiol. Scand.* **84**, 512–523.

FUNG, Y. C. (1969). Blood flow in the capillary bed. *J. Biomech.* **2**, 353–363.

GAEHTGENS, P., MEISELMAN, H. J., AND WAYLAND, H. (1970). Erythrocyte flow velocities in mesenteric microvessels of the cat. *Microvasc. Res.* **2**, 151–162.

HENRY, J. P., AND MEEHAN, J. P. (1971). "The Circulation," p. 16. Yearbook Medical Publishers, Inc., Chicago.

HUTCHINS, P. M., RAINS, T. D., AND GREENE, A. W. (1973). Microvascular reactivity to norepinephrine in the spontaneously hypertensive rat (ABS). *Microvasc. Res.* **6**, 123.

INTAGLIETTA, M., AND ZWEIFACH, B. W. (1971). Geometrical model of the microvasculature of rabbit omentum from in vivo measurements. *Circ. Res.* **28**, 593–600.

INTAGLIETTA, M., RICHARDSON, D. R., AND TOMPKINS, W. R. (1971). Blood pressure, flow, and elastic properties in microvessels of cat omentum. *Amer. J. Physiol.* **221**, 922–928.

LEW, H. S., AND FUNG, Y. C. (1970). Plug effect of erythrocytes in capillary blood vessels. *Biophys. J.* **10**, 80–99.

LIGHTHILL, M. J. (1968). Pressure forcing of tightly fitting pellets along fluid-filled elastic tubes. *J. Fluid Mech.* **34**, 113–43.

LIN, K. L., LOPEZ, L., AND HELLUMS, J. D. (1973). Blood flow in capillaries. *Microvasc. Res.* **5**, 7–19.

LIPOWSKY, H. H., AND ZWEIFACH, B. W. (1974). Network analysis of microcirculation of cat mesentery. *Microvasc. Res.* **7**, 73–83.

MAYROVITZ, H. N., NOORDERGRAAF, A., AND PETERSON, L. H. (1973). Control of pre-capillary sphincter dynamics (ABS). *The Physiologist* **16**, 391.

MAYROVITZ, H. N. (1974). The microcirculation: theory and experiment. Ph.D. dissertation, University of Pennsylvania.

NICOLL, P. A., AND WEBB, R. L. (1955). Vascular patterns and active vasomotion as determiners of flow through minute vessels. *Angiology* **6**, 291-310.

NOORDERGRAAF, A. N. (1969). Hemodynamics. In "Biological Engineering" (H. P. Schwan, ed.). pp. 391–545. McGraw-Hill Book Co., New York.

WIEDEMAN, M. P. (1962). Lengths and diameters of peripheral arterial vessels in the living animal. *Circ. Res.* **10**, 686–690.

WIEDEMAN, M. P. (1963). Dimensions of blood vessels from distributing artery to collecting vein. *Circ. Res.* **12**, 375–381.

WIEDEMAN, M. P. (1968). Blood flow through terminal arterial vessels after denervation of the bat wing. *Circ. Res.* **22**, 83–89.

WIEDERHIELM, C. A., AND WESTON, B. V. (1973). Microvascular, lymphatic, and tissue pressures in the unanesthetized mammal. *Amer. J. Physiol.* **225**, 992–996.